Simulation of Fused Deposition Modeling of Glass Fiber Reinforced ABS Impact Samples: The Effect of Fiber Ratio, Infill Rate, and Infill Pattern on Warpage and Residual Stresses

Berkay Ergene[1] Cagin Bolat[2]

[1]Pamukkale University, Mechanical Engineering, Denizli, Turkey
[2]Samsun University, Mechanical Engineering, Samsun, Turkey

ABSTRACT

It is known that products made of polymer materials or especially polymer materials with glass fiber and carbon fiber are used in many different areas such as automotive, aerospace, and defense. At this point, studies in the literature have gained momentum due to the combination of fiber-reinforced polymer materials emerging as a result of technological developments and industrial demands, and the fused deposition modeling (FDM) method providing the production of parts in desired sizes and complexity. Residual stresses and distortions occurring in polymer-based composite parts produced with FDM are among the problems that should be minimized. In this study, the influences of fiber ratio (%10, %15, and %20), infill rate (%20, %50, and %80), and infill pattern (line, honeycomb, and triangle) on the residual stresses and warpages generating in impact test specimens produced from glass fiber reinforced ABS filaments by fused deposition modeling were tried to be determined with the Digimat 2021 program. As a result of the findings, it was determined that the distortion values decreased and the thermal residual stress values went up with the increase in fiber ratio and infill rate. In addition, it can be reported that the distortions that bring out as a result of the separation of the produced parts from the production platform are caused by the high deformations condensing at the lower corner points of the parts.

Keywords:
Fused deposition modelling; Warpage; Residual stress; Infill rate; Fiber ratio

INTRODUCTION

In recent years, innovative and practical solutions have been put forward in many different branches of industry and technology due to the increasing competition in industrial manufacturing and the advanced engineering materials developed. In this context, studies on design improvements and special-purpose modifications related to traditional manufacturing methods such as casting, machining, welding, powder metallurgy, and plastic forming continue rapidly. At this point, the casting of particle-reinforced composites and foams for the aerospace and automotive industries (crash boxes and body elements) [1-3], micro-machining for biomedical implants, and macro-machining for hybrid composites [4, 5], different types of friction stir welding processes for the structural continuity of metals [6, 7], microwave and spark plasma sintering methods for composite and biomedical applications [8, 9], and simulation/model synthesis plastic forming processes [10, 11] are traditional methods coming to the fore in recent years.

Compared to conventional manufacturing techniques, additive manufacturing (AM), also known as three-dimensional (3D) printing technology, has become very popular in the last few years and has been researched in many different disciplines. Rapid prototyping capability, capacity to produce complex and difficult geometries, minimization of material waste, the practicality of application, low-cost system maintenance and repair, environmental friendliness, and compatibility with computer-aided automation can be emphasized as the main advantages of this technology [12-14]. Many different types of engineering materials, from polymer-based materials to metallic parts, from composite samples to ceramic-based products, can be produced according to computer-aided design procedures using AM

methods [15-18]. Although there are many different classification types in the technical literature for AM methods, the terminology in ASTM F42 and ISO TC 261 standards is generally used, including photopolymerization, powder bed melting, material extrusion, material jetting, binder jetting, sheet lamination, and direct energy deposition. Therefore, in the literature, there are seven basic categories in total [19, 20]. While the production of metals and composite parts with AM has increased over the last years, polymer materials are the most widely used materials in the field of AM due to both their low melting temperatures and high viscosity values. At this point, the fused deposition modelling (FDM) technique, in which polymer filaments are produced by layering on top of each other through nozzles according to the g-code created in the slicing program, stands out as the most preferred AM method.

Acrylonitrile butadiene styrene (ABS), polylactic acid (PLA), and polyethylene terephthalate glycol (PETG) are the most preferred filament polymers in the productions made via the FDM technique [21-27]. The viscous nature of these materials for printing, their low thermal expansion capabilities, and low melting temperatures provide advantages to manufacturers and prototype designers. When the studies in the scientific literature are examined in general terms; manufacturing optimizations, dimensional analyzes of the created product, and determination of correct manufacturing parameters are frequently encountered [28-35]. In addition to these issues, friction and wear analyzes are carried out for 3D-printed parts that need to work in contact under service conditions [36-39]. Also, fatigue tests are carried out to understand the damage mechanisms by testing the deformation that variable loadings will cause on the material depending on time [40-42]. In order to enhance the mechanical properties, post-manufacturing heat treatment or water absorption has been studied recently by researchers [43-46]. All these researches are very valuable and important in order to obtain an adequate and detailed engineering perspective on the basic mechanical and physical performances of the samples produced by the FDM technique.

In spite of the experimental studies in the technical literature providing significant information about the mechanical and physical properties of the final product, the detection of more complex features such as distortion and residual stress are carried out by computer-aided finite elements and simulation programs. By way of such AM-oriented software, researchers can avoid the trouble of installing expensive and complex test setups, while at the same time providing significant cost and time savings for future applications. For example; Syrlybayev et al. [47] performed distortion analysis on ABS tensile specimens produced with FDM using ANSYS software and suggested that increasing layer thickness led to a decrease in warpage. Lu et al. [48] used a finite element methodology to calculate the warpage amount of thin-walled Ti-6Al-4V samples fabricated by powder bed melting, and they found very close results with the analytical results. Similarly, Ergene [12] analyzed the residual stresses and temperature changes during additive manufacturing in biomedical parts that can be produced from Inconel 718 and Ti-6Al-4V materials by selective laser melting using the Amphyon 2021 program. Samy et al. [49] carried out both residual stress and distortion simulations for polypropylene (PP) sample formed with FDM and observed that when the ambient temperature increased from 25°C to 75°C, the thermal residual stresses in the parts decreased and the distortion increased. Ghnatios et al. [50] compared the amount of distortion in carbon fiber reinforced polyether ether ketone (PEEK) products produced by robotic printing technology with experimental and simulation methods. The researchers stated that the experimental results overlapped with the simulation results at the level of 89.8%. Bachhar et al. [51] analyzed numerically the amount of distortion caused by residual stresses occurring at the interface of the supporting pressure base and the final product in the PP samples. Moumen et al. [52] used the numerical simulation approach to optimize the FDM process parameters and showed in detail how the residual stresses and temperature distributions emerged throughout the part geometry. In another recent study, Zhang et al. [53] performed finite element analysis to determine the deformation and residual stress analysis on metal-based turbine blades produced by the laser melting technique. Huang et al. [54] compared different numerical solution methodologies for products formed by the wire and arc-fed AM method. The researchers suggested that the structural and adaptive node technique was up to nine times faster than the Abaqus software. Hajializadeh et al. [55] used the estimation method with artificial neural networks in addition to finite elements in the analysis of residual stresses in stainless steel products manufactured with AM and stated that the artificial intelligence integrated finite element technique was a very time-saving approach. Rouway et al. [56] compared distortion and residual stresses in polyamide (PA) and PEEK-based composite turbine blades using finite elements. According to the findings, while PA-based products were more resistant to warping, less residual stress was detected in PEEK-based samples. Clark et al. [57] applied the finite element approach based on MSc Digimat AM software to model the thermal dissipation that is effective in warping in ABS samples and showed that it was a very practical way compared to physical tools such as thermal cameras, image processing, and thermocouple.

In this study, which seeks to respond to the need in the technical literature and the demand in the industrial AM sectors targeting rapid production capacity, the distortion and residual stress analyses for glass fiber reinforced ABS

samples manufactured with FDM were performed numerically for the first time. By using finite elements and simulation techniques, the temperature distributions on the products were determined and the distribution of the deformation along the product geometry was examined. All analyzes of glass fiber reinforced ABS products with different volumetric ratios (10%, 15%, 20%) were made using the additive manufacturing module in the new generation and R&D-focused Digimat AM 2021 program. Furthermore, considering the serious effect on the product weight, the filling ratio values, which are one of the critical manufacturing parameters, were selected as 20%, 50%, and 80%. As final products, impact specimens that were created according to the ASTM 6110 were selected and three different filling patterns were appointed honeycomb, line, and triangle.

MATERIAL AND METHODS

The most common manufacturing defect in polymer products manufactured through FDM is warpage. This situation becomes very important, especially in the production of prototypes in precision dimensions. The basic mechanism of the warping problem is the successive accumulation of layers. This mechanism is followed by the effects of expansion and contraction due to the heating-cooling cycle causing different stresses on the product. Generally, the shrinkage effect that occurs with the contact of cold air from the top surface of the last layer, forces the product to be lifted from the manufacturing platform and the manufacturing platform-part connection is broken. In Fig. 1, the schematic view of the warpage event is shared.

In the study conducted by Armilotta et al. [58], the possible factors affecting the distortion are listed as follows;

a) Part geometry: length, width, and height

b) Material: Thermal expansion coefficient, elastic modulus, Poisson ratio, and glass transition temperature
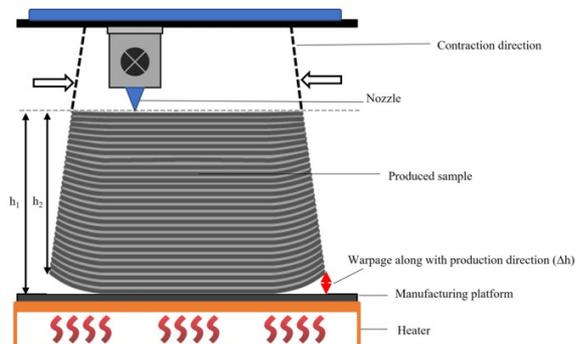
c) Process parameters: layer thickness, the temperature of the fabrication platform, printing speed, and the height of support material

In the methodology phase of this study, as also happened in another study in the literature [59], firstly, model designs were made according to ASTM D6110, which is used to determine the impact strength of plastic impact samples with notches. By looking at ASTM D6110, impact test specimens with a length of 80 mm, a width of 10 mm, and a thickness of 4 mm were designed in AutoCAD 2020 (Fig. 2a). Then, the model was saved in AutoCAD 2020 program with stl extension and transferred to the Repetier Host slicing program. Using the FDM parameters given in Table 1, the g-code of the three-dimensional part was created (Fig. 2b). Afterward, the design and g-code of the impact samples were transferred to the finite element-based Digimat AM 2021 program. In the Digimat AM 2021 program, the voxel structure and mesh size of 0.5 mm were assigned to the designed structures. The number of voxels used during the meshing process in the simulations varied between 26150 and 33250. Before deciding on the relevant mesh size, preliminary simulations were held with mesh sizes of 0.25 mm, 0.5 mm, 0.75 mm, 1 mm, and 2 mm.

Considering the values obtained as a result of mesh optimization, the mesh size was set as 0.5 mm. While no significant change was observed in the results at values below 0.5 mm mesh size, changes were detected in the simulation results with mesh sizes above 0.5 mm. With the AM simulations of mesh parts (Fig. 2c), it is desired to observe not only the distortion in the part but also the residual stresses and the temperatures that occur. In this direction, not only warping analyzes but also thermo-mechanical analyzes were performed according to the AM parameters entered in the slicer program.

After the transfer of the part to be simulated and the g-code to the Digimat AM 2021 program, glass fibers with an aspect ratio of 15 were added to the relevant models. Additionally, three different fiber ratios (10%, 15%, and 20%),

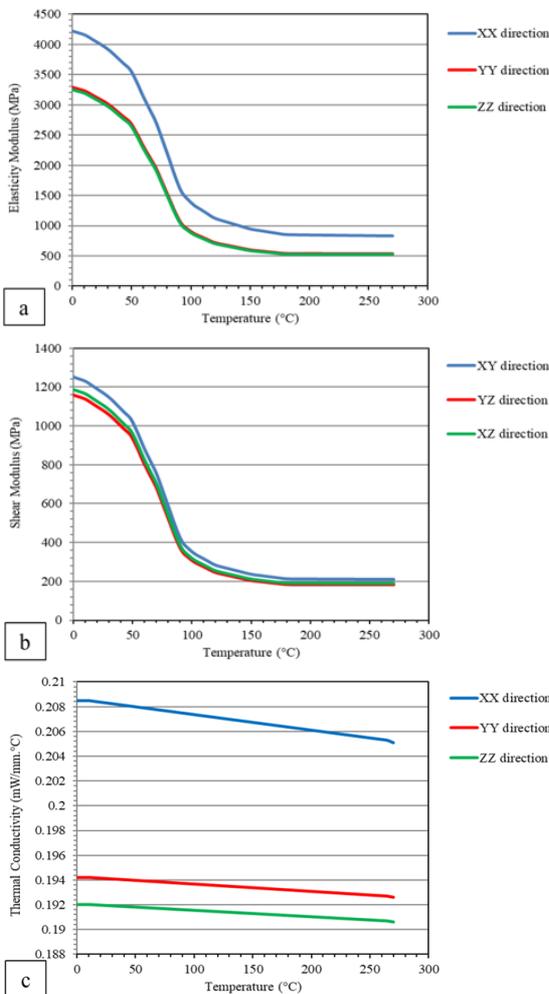**Figure 1.** Schematic view of warpage in manufacturing with FDM.
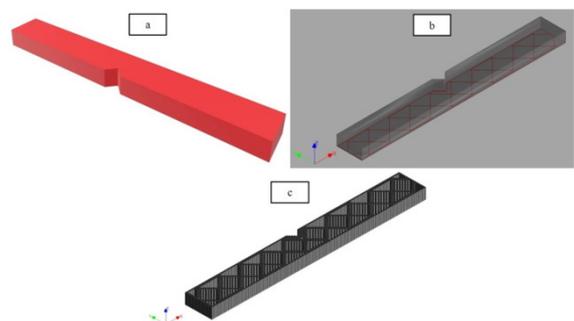
Figure 2. a) CAD model in accordance with ASTM D6110, b) tool path and g-code interface, c) and mesh structure as an example.
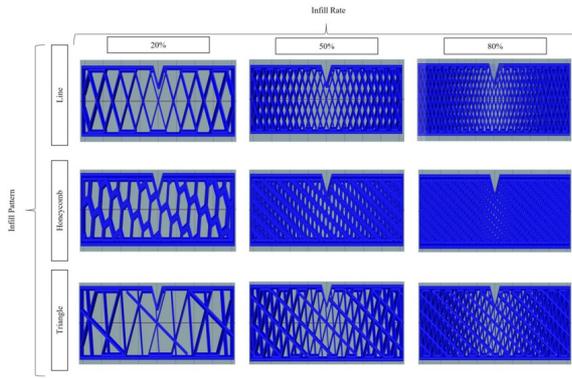
Figure 3. The appearance of the different infill patterns used during the simulations depending on the infill rate.

three different infill ratios (20%, 50%, and 80%), and three different filling patterns (line, honeycomb, triangle) were picked. Fig. 3 shows the images in the Repetier Host slicer program of the samples defined based on different fill patterns and fill rates. The material properties of each composite were calculated in the material library in the Digimat

Table 1. FDM parameters used during simulations.

Fabrication parameters	Values
Layer thickness (mm)	0.25
Layer width (mm)	0.35
Infill rate (%)	20/50/80
Infill pattern	Line/Honeycomb/Triangle
Number of contours	1
Fabrication angle (°)	45/-45
Platform temperature (°C)	115
Extrusion temperature (°C)	250
Room temperature (°C)	23
Nozzle diameter (mm)	0.4
Printing speed (mm/s)	50

AM 2021 program and exported from the relevant library. For example; some of the mechanical and thermal material properties of the composite structure with a glass fiber additive ratio of 10% are presented in Fig. 4. On the other side, as in other studies in the literature [47, 60, 61], some assumptions were made in this study. During the simulations; it is accepted that the ABS material used as the matrix material has a perfect microstructure, the glass fibers had the same properties along their geometry, the length/diameter ratio of all fibers is perfect and the same, and mechanisms such as creep that may occur at high temperatures are not taken into account, and the room temperature does not change.

RESULTS AND DISCUSSION

Effect of Fiber Ratio

Depending on the changing fiber ratio, the variation in the distortion data is shared in Fig. 5 for the 20% infill rate where the highest distortion occurs. According to the increased fiber content, a decreasing trend was observed in the distortion values for all three infill pattern types, and this trend was the same for all other infill rate levels, as determined from the simulation results. The

Figure 4. a) Changes of elasticity modulus, b) shear modulus, and c) thermal conductivity properties depending on temperature.
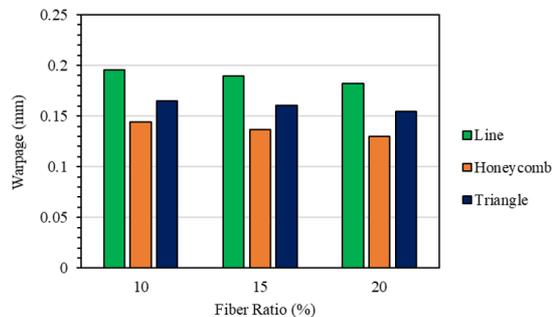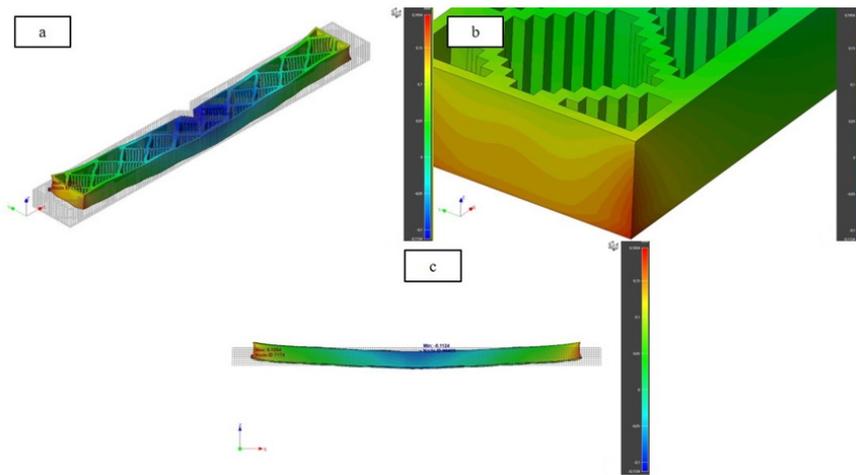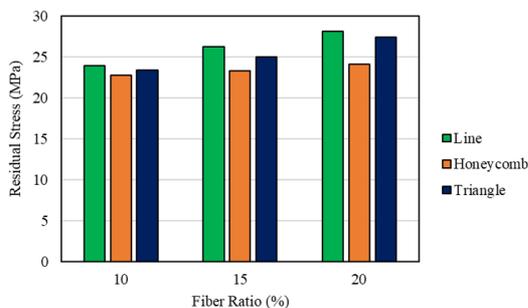

Figure 5. The effect of varying fiber ratio on warping for different infill patterns.

Figure 6. Warpage figures obtained from simulation results; a) 3D view, b) most warped corner joint, c) 2D view.

highest distortion value was found as 0.1954 mm for 10% fiber content, 20% infill rate, and line pattern parameters. In contrast, the lowest value of 0.0941 mm was recorded for 20% fiber content, 80% infill rate, and honeycomb pattern. As it is known from the technical literature [62, 63], as a result of increasing fiber ratio and mixing rule of composites, there is a direct correlation between elastic modulus/rigidity and ceramic reinforcement fiber ratio. This is an important reason for the reduced distortion, and the simulation results support this. In line with these findings, Dou et al. [64] reported that the tensile strength of additive fabricated polymer composites improved depending on the increasing fiber ratio. In addition, Korkees et al. [65] stated that the flexural strength of the composite test specimens was positively affected by the increase in the fiber ratio.

In Fig. 6, simulation images are given along the geometry of the part where the maximum distortion is observed. An upward lifting behavior was observed at all corners due to the shrinkage occurring because of the cooling, and the warping behavior in this direction. This situation was similarly repeated for all other manufacturing parameters. The risk of separation between the manufacturing platform and the manufactured part was observed at the outermost edges and corners. A distortion behavior similar to this cir-

cumstance has been reported by Syrlybayev et al. [47].

Fig. 7 shows the variation of residual stresses in post-manufacturing products depending on the fiber ratio and infill pattern, while the occupancy rate (20%, for the highest distortion) is constant. From this, it can be said that as the fiber ratio increases, the residual stresses in the additively manufactured composite products increase for all infill pattern types. This trend is similar to other manufacturing parameter combinations. Along with the increase in fiber ratio, the polymer-fiber contact surfaces in the composite system also get bigger along the entire product geometry. According to the data taken from the material library of the Digimat AM 2021 simulation program, there is a great difference between the thermal expansion coefficient of ABS material (90×10^{-6} 1/°C) and the thermal expansion coefficient of glass fibers (6×10^{-6} 1/°C), and the elongation/degree of ABS material tensile strength is higher.

After the final cooling, additional residual stresses occur in the matrix-fiber interface regions as a result of the shrinkage tendency of the ABS regions. For these reasons, there is a positive relationship between fiber ratio and residual stresses. Depending on the thermal cycle-based production method and the presence of phases with two different heat transfer coefficients in polymer-ceramic structure, Öz et al. [66] also found residual stresses in the interface regions of carbon fibers and epoxy matrix in their study where they performed residual stress analysis using the finite element method.

Warpage and Temperature Distribution During Manufacturing

By using Digimat AM 2021, the accumulation processes that additive manufacturing creates on the product depending on the layers can be examined in terms of both distortion amounts and temperature distributions. In this study, since the thickness of each layer is 0.25 mm,

Figure 7. The effect of varying fiber ratio on residual stress for different infill patterns.
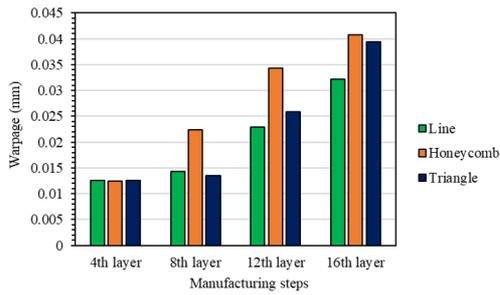
Figure 8. Warpage values that change according to production layers during additive manufacturing.
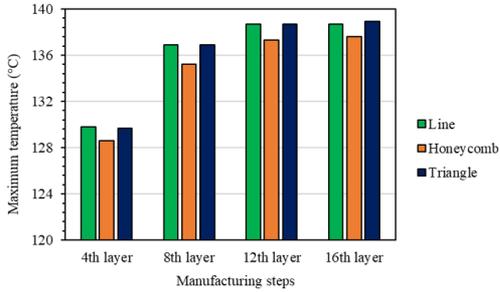
Figure 9. The highest temperature values that change according to the increasing layer numbers during additive manufacturing.

the product takes its final shape with a total of 16 layers. To examine the warpage and temperature changes that occur during the manufacturing step by step, data analysis was carried out in each of the four layers. Fig. 8 and Fig. 9, show the warpage and the highest temperature values depending on the number of layers increasing during manufacturing in the part for the 10% fiber content and 20% infill rate product, where the highest warpage is seen.

There is a positive interaction between the warpage results and the ascending number of layers. This is due to the successive new layers triggering the distortion effects

caused by the previously created ones. On the other hand, the highest temperatures on the parts go up with the increasing number of layers, regardless of the type of infill pattern. For the first created layers, the highest temperature values detected in the part range from 128.6 °C to 129.8°C due to the manufacturing platform temperature (115°C) which is lower than the printing temperature (250°C). With the continuation of the printing, the product approaches the temperature equilibrium with the effect of the new layers added. The highest temperatures with the last layer change between 137.6 °C (honeycomb) and 138.9°C (triangle) depending on the infill pattern type. As it can be understood from this temperature distribution, the part is exposed to shrinkage due to the temperature differences between the upper layers of the manufactured part and the layers close to the production platform. Then, the related part starts to lift from the corner points of the layers close to the production platform and results in warping. This is also confirmed in the geometric simulations for the highest distortion conditions given in Fig. 10 and Fig. 11. According to Fig. 11, regions with high temperatures are seen on the edge line. This phenomenon may be caused by the late cooling of the frame line.
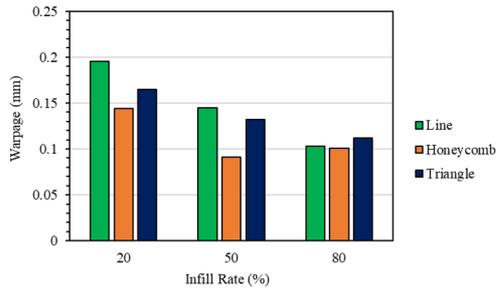
Effect of Infill Rate

Fig. 12 shows the amount of distortion on the manufactured products at a 10% fixed fiber ratio (for the highest warpage) depending on the varying infill rates and pattern types. When the results are analyzed, a significant decrease is noticed in distortion and this is the same for other fiber ratio levels. The adverse relationship between the amount of distortion and production infill rates can be largely explained by the total porosity level. As the void ratio in the manufactured parts increases, the amount of load-bearing column/support in the structural mesh goes down. This case reduces the tensile strength and
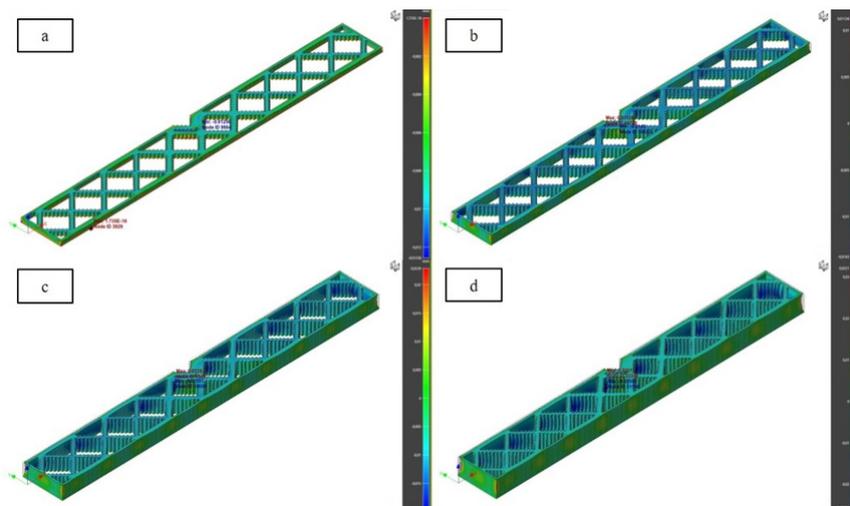

Figure 10. Warpage amounts in the product geometry, depending on the layers added during manufacturing; a) 4th layer, b) 8th layer, c) 12th layer, d) 16th layer.
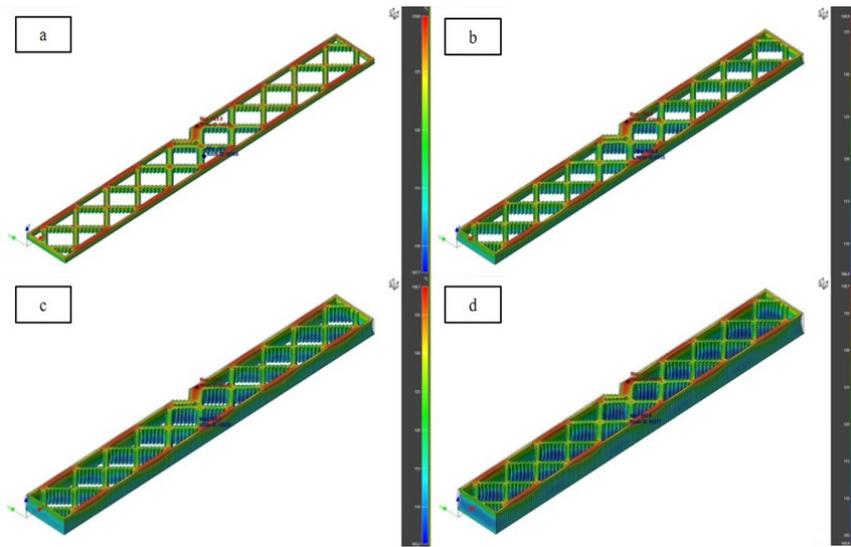
Figure 11. Temperature distributions in the product geometry depending on the layers added during manufacturing; a) 4th layer, b) 8th layer, c) 12th layer, d) 16th layer.

**Figure 12.** The effect of varying infill rate on warpage for different infill patterns.
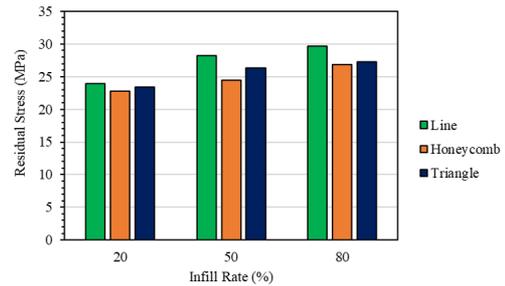
Figure 13. The effect of varying infill rate on residual stress values for different infill patterns.

elastic modulus values of the products. On the other side, as the infill ratio increases, the distortion values decrease owing to the lowering pore level. Similar findings in which the mechanical properties of ceramic fiber-filled polymer composites produced with FDM improved due to the increasing fill rate levels were emphasized in the study by Öteyaka et al. [67].

There is a directly proportional relationship between residual stresses and occupancy rate. This result can be explained by the extra polymer-glass fiber contact region within the structural mesh pattern. Fig. 13 shows the variation of residual stresses in fabricated parts at a 10% fixed fiber ratio (for highest distortion) for different infill ratios and infill pattern shapes. Similar behavior was found for other parameter clusters. Similar to the situation with the fiber ratio given in Fig. 7, it is thought that the internal stresses due to the shrinkage effects at the glass fiber-ABS contact points cause a higher level of residual stress in products with a high fill ratio. In addition, for all of the infill patterns, the stress-increasing trend due to the infill rate continues.

When the entire data set obtained with Digimat AM 2021 is analyzed; the highest residual stress value was found as 39.26 MPa for 20% fiber content, 80% infill rate, and line pattern parameters. The lowest value was calculated as 22.77 MPa for 10% fiber content, 20% infill rate, and honeycomb filling pattern. The simulation pictures showing the thermal residual stress distributions obtained along the ge-
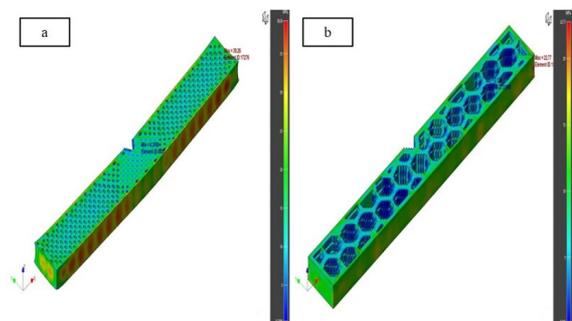
Figure 14. Thermal residual stress distributions along the part geometry; a) highest value line pattern sample, b) lowest value honeycomb pattern sample.

ometry of the part, specific to the highest and lowest values, are given in detail in Fig. 14a and Fig. 14b.

In addition to the values obtained as a result of the final cooling, the residual stresses during each layer set can also be followed through the Digimat AM 2021 program, which is specialized to analyze the additive manufacturing properties of composite materials. In this way, it is possible to analyze the product gradually during the manufacturing process. For the model given in Figure 14a where the highest residual stress was recorded, the residual stresses in the first four, eight, twelve, and sixteenth layers were calculated as 12.9, 15.7, 20.9, and 25.2 MPa, respectively. This is a consequence of the combined effect of the number of thermal cycles and the increasing number of layers on the total stress. In the model given in Figure 14b, where the lowest residual stress was determined, the values of 10.1, 12.8, 16.8, and 20.2 MPa were read for the same layer increase groups.

At the end of obtaining all simulation results, as mentioned earlier the highest distortion value of 0.1954 mm was observed in the sample produced with 10% fiber content, 20% infill rate, and line pattern. To validate the simulation results, the three samples showing the maximum distortion according to simulation results were also 3D printed. The 3D printing process of the samples was performed by using 10% glass fiber reinforced ABS filament (FibreX ABS-GF10) and Ultimaker S3 model 3D printer in accordance with manufacturing parameters tabulated in Table 1. 3D printed

Figure 15. Validation of the simulation results with 3D printed sample; a) 3D printed samples, b) Warpage measurements.

Table 2. Comparison of the experimental and simulation results in terms of warpage.

| Sample No	Experimental warpage result (mm)	Simulation warpage result (mm)	Accuracy between simulation and experiments (%)
1	0.19	0.1954	97.23
2	0.21		93.04
3	0.21		93.04

validation samples and their validation process were given in Fig. 15a and Fig. 15b respectively. In addition, validation results were shared in Table 2 below. As can be understood from Table 2, accuracy between simulation and experimental results for warpage ranged between 93.04% and 97.23%. In addition, when the literature efforts were scanned, Armilotta et al. [58] focused on the warpage of the ABS parts fabricated with the FFF method and expressed that warpage values ranged between 0.17 mm and 1.07 mm depending on the geometrical features. Besides, in another study, Syrlybayev et al. [47] performed a study on warpage analysis of ABS parts and according to measured warpage values via digital caliper, the result varied between 0.59 and 0.89 mm. At this point, the results obtained in our study can be evaluated as lower than the pure ABS and this situation can be attributed to the reinforcement glass ceramic fibers triggering the total rigidity rising.

CONCLUSION

In the light of the numerical calculations performed on glass fiber reinforced ABS models so as to find warpage and residual stress properties, the following can be listed;

• Apart from the frequently tried polymeric materials, ceramic fiber reinforced polymer samples can be analyzed and modeled in point of warpage via Digimat AM software.

• As long as the fiber content escalates in the samples, warpage amounts drop with increasing rigidity regardless of the infill pattern.

• Warpage of the specimens decreases together with the rising of the infill ratio.

• As a result of body simulations, the most deformed sections are the edges and corners of the models.

• Thanks to software with special purpose additive manufacturing, the fabrication process can be planned according to stages and the temperature of the final product can be monitored layer by layer.
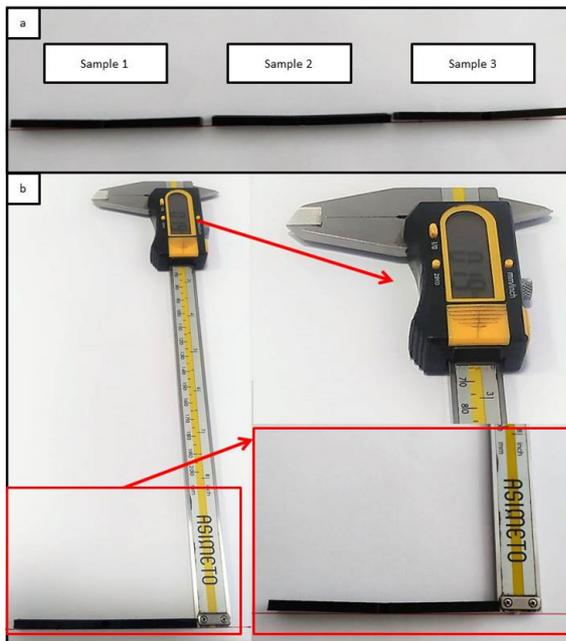
- There is a positive interaction between the residual stresses and infill ratio and the fiber ratio induces extra thermal stresses.
- The highest residual stress levels are read for line-patterned models whereas the lowest values belong to the models created with honeycomb pattern.

CONFLICT OF INTEREST

Authors approve that to the best of their knowledge, there is not any conflict of interest or common interest with an institution/organization or a person that may affect the review process of the paper.

AUTHOR CONTRIBUTION

Berkay Ergene: Conceptualization, Investigation, Method-ology, Resources, Simulations, Analysis, Writing-Original Draft, Review&Editing; **Cagin Bolat:** Methodology, Resources, Simulations, Analysis, Writing-Review&Editing

REFERENCES

1. Mandloi P., Dhakar B., Pare V. and Manepatil S. Experimental investigation of wear properties of AA6061 + Al2O3 metal matrix composite fabricated by vacuum stir casting method, Mater. Today-Proc, 61 (1) (2022) 55-61.

2. Bolat Ç., Akgün İ.C. and Gökşenli A. Effects of particle size, bimodality and heat treatment on mechanical properties of pumice reinforced aluminum syntactic foams produced by cold chamber die casting, China Foundry, 18 (2021) 529-540.

3. Bolat Ç., Bilge G. and Gökşenli A. An investigation on the effect of heat treatment on the compression behavior of aluminum matrix syntactic foam fabricated by sandwich infiltration casting, Mat. Res., 24 (2) (2021).

4. Davis R., Singh A., Debnath K., Sabino R.M., Popat,K., Soares P., Keshri A.K. and Borgohain B. Enhanced micro-electric discharge machining-induced surface modification on biomedical Ti-6Al-4V alloy, ASME. J. Manuf. Sci. Eng., 144 (7) (2022).

5. Ergene B. and Bolat Ç. A review on the recent investigation trends in abrasive waterjet cutting and turning of hybrid composites, Sigma Journal of Engineering and Natural Sciences, 37 (3) (2019) 989-1016.

6. Ünal E., Karaca F. and Sarsılmaz F. Investigation of interface microstructure properties of AISI 316l /AISI 4140 steel couple welded by friction welding process, Journal of the Faculty of Engineering and Architecture of Gazi University, 34 (2) (2019) 701-708.

7. Mahdianikhotbesara A., Sehhat M.H. and Hadad M. Experimental study on micro-friction stir welding of dissimilar butt joints between Al 1050 and pure copper., Metallogr. Microstruct. Anal., 10 (2021) 458-473.

8. Annur D., Rochmanto F., Thaha Y.N., Kartika I., Dimyati A. and Supriadi S. Processing and characterization of porous titanium for orthopedic implant prepared by argon-atmospheric sintering and arc plasma sintering, Mat. Res., 24 (6) (2021).

9. Wang Z., Xu L., Peng J., Tang Z., Han Z. and Liu J. Effect of the microstructure and properties of graphite/copper composites fabricated by microwave sintering. J. Mater. Sci., 56 (2021) 9183-9195.

10. Nasiri S., Sadegh-Yazdi M., Mousavi S.M., Ziya-Shamami M. and Mostofi T.M. Repeated underwater explosive forming: Experimental investigation and numerical modeling based on coupled Eulerian–Lagrangian approach, Thin. Wall. Struct., 172 (2022).

11. Bhujangrao T., Veiga F., Penalva M., Costas A. and Ruiz C. (2022). Three-dimensional finite element modelling of sheet metal forming for the manufacture of pipe components: Symmetry considerations, Symmetry, 14 (2022) 228.

12. Ergene B. Simulation of the production of Inconel 718 and Ti6Al4V biomedical parts with different relative densities by selective laser melting (SLM) method, Journal of the Faculty of Engineering and Architecture of Gazi University, 37 (1) (2022) 469-484.

13. Ravikumar P., Desai C., Kushwah, S. and Mangrola M.H. A review article on FDM process parameters in 3D printing for composite materials, Mater. Today. Proc., 60 (3) (2022) 2162-2166.

14. Yoo S.Y., Kim S.K., Heo S.J., Koak J.Y. and Kim J.G. Dimensional accuracy of dental models for three-unit prostheses fabricated by various 3D printing Technologies, Materials, 14 (2021) 1550.

15. Liu Z., Wang Y. and Wu B. A critical review of fused deposition modeling 3D printing technology in manufacturing polylactic acid parts, Int. J. Adv. Manuf. Technol., 102 (2019) 2877-2889.

16. Kumar, S. and Kishor, B. Ultrasound Added Additive Manufacturing for Metals and Composites: Process and Control. In: Mavinkere Rangappa, S., Gupta, M.K., Siengchin, S., Song, Q. (eds) Additive and Subtractive Manufacturing of Composites. Springer Series in Advanced Manufacturing (2021) Springer, Singapore.

17. Zhang H., Huang T., Jiang Q., He L., Bismarck A. and Hu Q. Recent progress of 3D printed continuous fiber reinforced polymer composites based on fused deposition modeling: a review, J. Mater. Sci., 56 (2021) 12999-13022.

18. Carloni D., Zhang G. and Wu Y. Transparent alumina ceramics fabricated by 3D printing and vacuum sintering, J. Eur. Ceram. Soc., 41 (2021) 781-791.

19. Gibson, I., Rosen, D., Stucker, B. and Khorasani, M. Additive Manufacturing Technologies 3rd Edition, Springer, New York,(2021).

20. Beaman J.J., Bourell D.L., Seepersad C.C. and Kovar D. Additive manufacturing review: Early past to current practice, ASME. J. Manuf. Sci. Eng., 142 (11) (2020).

21. Solomon I.J., Sevvel, P. and Gunasekaran J. A review on the various processing parameters in FDM, Mater. Today. Proc., 37 (2) (2021) 509-514.

22. Popescu D., Zapciu A., Amza C., Baciu F. and Marinescu M. FDM process parameters influence over the mechanical properties of polymer specimens: A review, Polymer Testing, 69 (2018) 157-166.

23. Syrlybayev D., Zharylkassyn B., Seisekulova A., Akhmetov M., Perveen A. and Talamona D. Optimisation of strength properties of FDM printed parts—A critical review, Polymers, 13 (2021) 1587.

24. Özen A., Abali B.E., Völlmecke C., Gerstel J. and Auhl D. Exploring the role of manufacturing parameters on microstructure and mechanical properties in fused deposition modeling (FDM) using PETG, Appl. Compos. Mater., 28 (2021) 1799-1828.

25. Karabeyoglu S.S., Eksi O., Yaman P. and Kucukyildirim B.O. Effects of infill pattern and density on wear performance of FDM-printed acrylonitrile-butadiene-styrene parts, J. Polym. Eng., 41 (2021) 854-862.

26. Ergene B., Atlıhan G. and Pinar A. Investigation of the effect of taper angle and boundary condition on natural frequency of the 3D

printed PET-G beams, Int. J. Print. Technol. Digit. Ind., 6 (2022) 31-39.

27. Karabeyoglu S.S., Eksi O., Istif I. and Feratoglu K. Identification of tensile behaviour of polylactic acid parts manufactured by fused deposition modeling under heat-treated conditions using nonlinear autoregressive with exogenous and transfer function models, J. Polym. Eng., 42 (2022) 1004-1016.

28. Mercado-Colmenero J.M., La Rubia M.D., Mata-Garcia E., Rodriguez-Santiago M. and Martin-Doñate C. Experimental and numerical analysis for the mechanical characterization of PETG polymers manufactured with FDM technology under pure uniaxial compression stress states for architectural applications, Polymers, 12 (2020) 2202.

29. Srinivasan R., Nirmal Kumar, K., Jenish Ibrahim A., Anandu, K.V. and Gurudhevan R. Impact of fused deposition process parameter (infill pattern) on the strength of PETG part, Mater. Today. Proc., 27 (2) (2020) 1801-1805.

30. Sehhat M.H., Mahdianikhotbesara A. and Yadegari F. Impact of temperature and material variation on mechanical properties of parts fabricated with fused deposition modeling (FDM) additive manufacturing, Int. J. Adv. Manuf. Technol., 120 (2022) 4791-4801.

31. Nathaphan S. and Trutassanawin W. Effects of process parameters on compressive property of FDM with ABS, Rapid Prototyping J., 27 (5) (2021) 905-917.

32. Vyavahare S. and Kumar S. Numerical and experimental investigation of FDM fabricated re-entrant auxetic structures of ABS and PLA materials under compressive loading, Rapid Prototyping J., 27 (2) (2021) 223-244.

33. Algarni M. and Ghazali S. Comparative study of the sensitivity of PLA, ABS, PEEK, and PETG's mechanical properties to FDM printing process parameters, Crystals, 11 (2021) 995.

34. Chokshi H., Shah D.B., Patel K.M. and Joshi S.J. Experimental investigations of process parameters on mechanical properties for PLA during processing in FDM, Adv. Mater. Process. Technol., (2021). 1-14.

35. Ergene B., Şekeroğlu İ., Bolat Ç, and Yalçın B. An experimental investigation on mechanical performances of 3D printed lightweight ABS pipes with different cellular wall thickness, J. Mech. Eng. Sci., 15 (2) (2021) 8169-8177.

36. Norani M.N.M., Abdollah M.F.B., Abdullah M.I.H.C., Amiruddin H., Ramli F.R. and Tamaldin N. 3D printing parameters of acrylonitrile butadiene styrene polymer for friction and wear analysis using response surface methodology, P I MECH ENG J-J ENG., 235 (2) (2021) 468-477.

37. Raheja K., Jain A., Sharma C., Rana R. and Lal R. Comparative Study of Tribological Parameters of 3D Printed ABS and PLA Materials. In: Singari, R.M., Mathiyazhagan, K., Kumar, H. (eds) Advances in Manufacturing and Industrial Engineering. Lecture Notes in Mechanical Engineering. (2021) Springer, Singapore

38. Phogat A., Chhabra D., Sindhu V. and Ahlawat A. Analysis of wear assessment of FDM printed specimens with PLA, multi-material and ABS via hybrid algorithms, Mater. Today., 62 (1) (2022) 37-43.

39. Ergene B. and Bolat Ç. An experimental study on the role of manufacturing parameters on the dry sliding wear performance of additively manufactured PETG, Int. Polym. Process., 37 (3) (2022) 255-270.

40. Safai L., Cuellar J.S., Smit G. and Zadpoor A.A. A review of the fatigue behavior of 3D printed polymers, Addit. Manuf., 28 (2019) 87-97.

41. Azadi M., Dadashi A., Dezianian S., Kianifar M., Torkaman S. and Chiyani M. High-cycle bending fatigue properties of additive-manufactured ABS and PLA polymers fabricated by fused

deposition modeling 3D-printing, Forces in Mechanics, 3 (2021).

42. Magri A., Vanaei S., Shirimbayan M., Vaudreuil S. and Tchakhtchi A. An Investigation to Study the Effect of Process Parameters on the Strength and Fatigue Behavior of 3D-Printed PLA-Graphene, Polymers, 13 (19) (2021) 3218.

43. Basgul C., Yu T., MacDonald D.W., Siskey R., Marcolongo M. and Kurtz S.M. Does annealing improve the interlayer adhesion and structural integrity of FFF 3D printed PEEK lumbar spinal cages?, J Mech Behav Biomed Mater., 102 (2020) 103455.

44. Akhoundi B., Nabipour M., Hajami F. and Shakoori D. An Experimental Study of Nozzle Temperature and Heat Treatment (Annealing) Effects on Mechanical Properties of High-Temperature Polylactic Acid in Fused Deposition Modeling, Polym Eng Sci., 60 (2020) 979-987.

45. Kumar K.S., Soundararajan R., Shanthosh G., Saravanakumar P. and Ratteesh M. Augmenting effect of infill density and annealing on mechanical properties of PETG and CFPETG composites fabricated by FDM, Mater. Today, 45 (2) (2021) 2186-2191.

46. Mishra K.P., Ponnusamy S. and Nallamilli, M.S.R. The influence of process parameters on the impact resistance of 3D printed PLA specimens under water-absorption and heat-treated conditions, Rapid Prototyp. J., 27 (6) (2021) 1108-1123.

47. Syrlybayev D., Zharylkassyn B., Seisekulova A., Perveen A. and Talamona D. Optimization of the Warpage of Fused Deposition Modeling Parts Using Finite Element Method, Polymers, 13 (2021) 3849.

48. Lu X., Chiumenti M., Cervera M., Tan H., Lin X. and Wang S. Warpage Analysis and Control of Thin-Walled Structures Manufactured by Laser Powder Bed Fusion, Metals, 11 (2021) 686.

49. Samy A.A., Golbang A., Harkin-Jones E., Archer E., Tormey D. and McIlhagger A. Finite element analysis of residual stress and warpage in a 3D printed semi-crystalline polymer: Effect of ambient temperature and nozzle speed, J. Manuf. Process., 70 (2021) 389-399.

50. Ghnatios C. and Fayazbakhsh K. Warping estimation of continuous fiber-reinforced composites made by robotic 3D printing, Addit. Manuf., 55 (2022) 102796.

51. Bachhar N., Gudadhe A., Kumar A., Andrade P. and Kumaraswamy G. 3D printing of semicrystalline polypropylene: towards eliminating warpage of printed objects. Bull Mater Sci, 43 (2020) 171.

52. Moumen A.E., Tarfaoui M. and Lafdi K. Modelling of the temperature and residual stress fields during 3D printing of polymer composites. Int J Adv Manuf Technol, 104 (2019) 1661–1676.

53. Zhang Y., Li F. and Jia D. Residual stress and deformation analysis of lattice compressor impeller based on 3D printing simulation, Mech. Adv. Mater. Struct., 29 (5) (2022) 717-731.

54. Huang H., Ninshu M., Chen J., Feng Z. and Murakawa H. Toward large-scale simulation of residual stress and distortion in wire and arc additive manufacturing, Addit. Manuf., 34 (2020) 101248.

55. Hajializadeh F. and Ince A. Integration of artificial neural network with finite element analysis for residual stress prediction of direct metal deposition process, Mater. Today Commun., 27 (2021) 102197.

56. Rouway M., Nachtane M., Tarfaoui M., Chakhchaoui N., Omari L. E.H., Fraija F. and Cherkaoui O. 3D printing: rapid manufacturing of a new small-scale tidal turbine blade. Int J Adv Manuf Technol., 115 (2021) 61–76.

57. Clark S., Yap T. and Tehrani M. Validation of a Finite Element Model for Fused Filament Fabrication Additive Manufacturing, Proceedings of the ASME 2021 International Mechanical Engineering Congress and Exposition. Volume 2A: Advanced Manufacturing. Virtual, Online. November 1–5, (2021).

58. Armilotta A., Bellotti M. and Cavallaro M. Warpage of FDM parts:

Experimental tests and analytic model. Robot Comput Integr Manuf., 50 (2018) 140-152.

59. Caminero M.A., Chacón J.M., García-Moreno I. and Rodríguez G.P. Impact damage resistance of 3D printed continuous fibre reinforced thermoplastic composites using fused deposition modelling, Compos. B. Eng., 148 (2018) 93-103.

60. Xinhua L., Shengpeng L., Zhou L., Xianhua Z., Xiaohu C. and Zhongbin W. An investigation on distortion of PLA thin-plate part in the FDM process, Int. J. Adv. Manuf. Technol., 79 (2015) 1117-1126.

61. Huynh T.T., Nguyen T.V.T., Nguyen Q.M. and Nguyen T.K. Minimizing warpage for macro-size fused deposition modeling parts, CMC Comput. Mater. Contin., 68 (2021) 2913-2923.

62. Kaw A.K. Mechanics of Composite Materials, 2nd ed. USA, Taylor and Francis, (2006).

63. Yalçın B. and Ergene B. Analyzing the Effect of Crack in Different Hybrid Composite Materials on Mechanical Behaviors, Pamukkale University Journal of Engineering Sciences, 24 (4) (2018) 616-625.

64. Dou H., Cheng Y., Ye W., Zhang D., Li J., Miao Z. and Rudykh S. Effect of process parameters on tensile mechanical properties of 3D printing continuous carbon fiber-reinforced PLA composites, Materials, 13 (2020) 3850.

65. Korkees F., Allenby J. and Dorrington P. 3D printing of composites: design parameters and flexural performance, Rapid Prototyping J., 26 (4) (2020) 699-706.

66. Öz F.E., Cinar K. and Ersoy N. Micromechanical progressive damage model for predicting resin dominated strength values of fibre reinforced composites under various types of loading, (2012) ECCM 2012 - Composites at Venice, Proceedings of the 15th European Conference on Composite Materials, June 24–28

67. Öteyaka M.Ö., Aybar K. and Öteyaka H.C. Effect of infill ratio on the tensile and flexural properties of unreinforced and carbon fiber-reinforced polylactic acid manufactured by fused deposition modeling, J. of Materi. Eng. and Perform. 30 (2021) 5203-5215.